Astronomy & Astrophysics manuscript no. sramirez˙msgms04˙arxiv
May 20, 2014
© ESO 2014

arXiv:1405.4494v1 [astro-ph.GA] 18 May 2014

Masgomas-4: Physical characterization of a double-core obscured cluster with a massive and very young stellar population.

S. Ramírez Alegría[1,2], A. Marín-Franch[3], and A. Herrero[4,5]

[1] The Millennium Institute of Astrophysics (MAS), Santiago, Chile.
[2] Instituto de Astrofísica, Universidad de Valparaíso, Valparaíso, Chile. e-mail: sebastian.ramirez@uv.cl
[3] Centro de Estudios de Física del Cosmos de Aragón (CEFCA), E-44001, Teruel, Spain. e-mail: amarin@cefca.es
[4] Instituto de Astrofísica de Canarias, 38205 La Laguna, Tenerife, Spain. e-mail: ahd@iac.es
[5] Departamento de Astrofísica, Universidad de La Laguna, E-38205 La Laguna, Tenerife, Spain.

Received 2013 / Accepted:

ABSTRACT

Context. The discovery of new, obscured massive star clusters has changed our understanding of the Milky Way star-forming activity from a passive to a very active star-forming machine. The search for these obscured clusters is strongly supported by the use of all-sky, near-IR surveys.
Aims. The main goal of the MASGOMAS project is to search for and study unknown, young, and massive star clusters in the Milky Way, using near-IR data. Here we try to determine the main physical parameters (distance, size, total mass, and age) of Masgomas-4, a new double-core obscured cluster.
Methods. Using near-IR photometry (J, H, and K_S) we selected a total of 21 stars as OB-type star candidates. Multi-object, near-IR follow-up spectroscopy allowed us to carry out the spectral classification of the OB-type candidates.
Results. Of the 21 spectroscopically observed stars, ten are classified as OB-type stars, eight as F- to early G-type dwarf stars, and three as late-type giant stars. Spectroscopically estimated distances indicate that the OB-type stars belong to the same cluster, located at a distance of $1.90^{+1.28}_{-0.90}$ kpc. Our spectrophotometric data confirm a very young and massive stellar population, with a clear concentration of pre-main-sequence massive candidates (Herbig Ae/Be) around one of the cluster cores. The presence of a surrounding H II cloud and the Herbig Ae/Be candidates indicate an upper age limit of 5 Myr.

Key words. Infrared: stars - Stars: early-types, massive - Techniques: photometric, spectroscopic - Open clusters and associations: Masgomas-4.

1. Introduction

Massive stars affect the interstellar medium at several scales (by ionizing their surrounding media, depleting their native clouds through their own birth, or modifying the star formation rate in their neighbourhood), and are fundamental pieces in Galactic evolution (Martins et al. 2005). Their influence on the Galaxy takes place during their very short periods, compared with less massive stars lifetimes. We often find them deeply embedded in their natal obscured massive clusters.

Owing to high-extinction in the Galactic plane, the detection of distant Galactic massive stars and clusters using optical data becomes impossible. Near-infrared photometric surveys such as 2MASS (Skrutskie et al. 2006), GLIMPSE (Benjamin et al. 2003), UKIDSS (Lawrence et al. 2007), and the ESO public survey VISTA Variables in the Vía Láctea (VVV, Minniti et al. 2010; Saito et al. 2012) have allowed the discovery of candidates in the Galaxy: for example Bica et al. (2003a,b), Dutra et al. (2003), and Froebrich et al. (2007) using 2MASS photometry; Davies et al. (2011), Kurtev et al. (2008), Kurtev et al. (2007), and Mercer et al. (2005) from GLIMPSE data; and Borissova et al. (2011) from Vista-VVV data.

Nevertheless, the census of massive clusters is far from complete; up to 100 clusters with masses greater than 10^4 $M_\odot$ may remain hidden (Hanson & Popescu 2008). Systematic search programmes for these objects are necessary for a full understanding of our Galaxy. This has motivated us to develop the MASGOMAS project (Marín-Franch et al. 2009). The present phase of the project is a systematic search for massive cluster candidates in the Galactic disc. Using the preliminary version of the search algorithm we found two new massive cluster candidates in the direction of the Scutum–Centaurus arm base. This very interesting region in the Milky Way hosts a concentration of massive clusters with a red supergiant population: RSGC1 (Figer et al. 2006), RSGC2 (Davies et al. 2007), RSGC3 (Alexander et al. 2009; Clark et al. 2009), Alicante 7 (Negueruela et al. 2011), Alicante 8, (Negueruela et al. 2010), and Alicante 10 (González-Fernández & Negueruela 2012). Our first cluster discovered in this direction, Masgomas-1 (Ramírez Alegría et al. 2012), is a spectroscopically confirmed massive cluster with an initial total mass of $(1.94 \pm 0.28) \cdot 10^4 M_\odot$ and a coexisting population of OB-type and RSG stars.

A second cluster candidate, Masgomas-4, is located in the coordinates $l = 40.530°$, $b = +2.576°$, or $\alpha_{2000} = 18^h56^m07^s$, $\delta_{2000} = +07°56'07''$. The candidate is found embedded a bright mid-IR nebulosity, as shown in Figure 1. Two IRAS sources are located close to Masgomas-4: IRAS 18536+0753 and IRAS 18537+0749. Their positions are also presented in Figure 1.

Based on these IRAS sources, we define two regions for Masgomas-4: region A (centred around IRAS 18536+0753) and region B (centred around IRAS 18537+0749). These regions have been extensively investigated in radio wavelength, but there

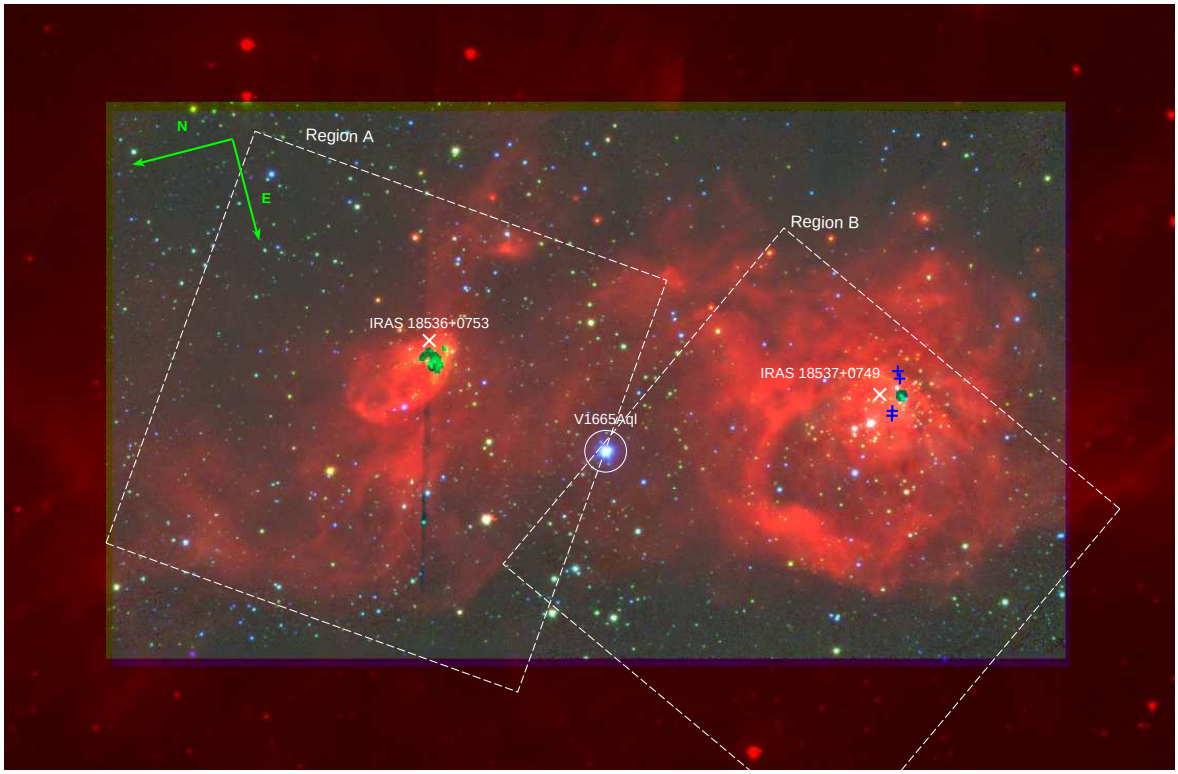

Fig. 1. Masgomas-4 false colour image (J=blue, K_S=green, 5.8 μm=red). J and K_S images are from LIRIS, and the 5.8 μm image is from IRAC, Spitzer. The size of Spitzer image is $12' \times 7'$, and the size of the false colour image is $9.2' \times 5.2'$. White crosses show the central positions of the IRAS sources and blue crosses show the position of the masers (water, ammonia, and methanol) reported in Section 1. The variable object V 1665 Aql is marked with a white circle. The arrows indicate the image orientation and are 1 arcminute in length. White squares show the orientation of both multi-object masks (masks A and B).

are no studies of their stellar population[1]. In region A we can find methanol (Slysh et al. 1999; Szymczak et al. 2000) and hydroxyl (Baudry et al. 1997) masers, both indicative of possible massive star formation. No distance estimates are available in the literature for region A.

In region B we find the H II region Sh2-76 E (Sharpless 1959; Zinchenko et al. 1997), which can also be associated with methanol and ammonia masers. For Sh2-76 E there are two distance estimates: one of 2.1 kpc, obtained by Plume et al. (1992) using water maser observations, and a second estimate of 2.2 kpc by Val'tts et al. (2000), using methanol maser observations ([HHG86] 185345.9+074916). The source Sh2-76 is also linked with the previously mentioned IRAS source IRAS 18537+0749. Chan et al. (1996, 1995) report it as a massive young stellar object and cite two distance estimates: 2.1 kpc (Zinchenko et al. 1994) and 2.33 kpc (Palagi et al. 1993).

In spite of the evidence of massive star formation in both regions A and B, there are no works dedicated to the observation and characterization of their stellar population. There is only a spectral classification of B7–9 V (Ibanoğlu et al. 2007) for V 1665 Aql, an eclipsing binary located between regions A and B. This binary system can be identified as a bright and blue source, with $K_S = 7.7$ mag and $(J - K_S) \sim 0$ mag, and according to Ibanoğlu et al. (2007), it is located at a distance of 477 pc. We will show later that this implies that the eclipsing binary is a foreground object.

[1] An optical spectrophotometric study by Forbes (1989) included five stars from the Masgomas-4 field. Spectral classification was reported only for one B7 V star, but the author does not associate this star with the H II region.

Because there are no previous works dedicated to its stellar population, we cannot state whether Masgomas-4 is a single cluster or both regions A and B are two different objects. We expect to solve this question by using the individual distance and extinction estimates. In either case, we will also carry out a complete physical characterization (mass, age, star formation activity) of both regions.

In this article we describe the near-IR observations of Masgomas-4 (Section 2) and the near-IR photometric diagrams and spectral classifications of the 21 spectroscopically observed stars (Section 3). In Section 4 we complete an analysis of the physical parameters (distance for individual regions, cluster distance, mass, and age), and we try to determine whether Masgomas-4 is a single cluster or two different objects. We summarize our results in Section 5.

2. Observations

We use data obtained with the LIRIS instrument (Manchado et al. 2004), a near-infrared imager/spectrograph mounted at the Cassegrain focus of the 4.2 m William Herschel Telescope (La Palma, Canary Island, Spain). The camera is equipped with a Hawaii 1024×1024 HgCdTe array detector, with a field of view of $4.2' \times 4.2'$ and a spatial scale of $0''.25$ pixel^{-1}. This work includes broadband near-infrared imaging using filters J ($\lambda_C = 1.250$ μm, $\Delta\lambda = 0.160$ μm), H ($\lambda_C = 1.635$ μm, $\Delta\lambda = 0.290$ μm), and K_S ($\lambda_C = 2.150$ μm, $\Delta\lambda = 0.320$ μm), and multi-object mid-resolution $R \sim 2500$ near-infrared spectroscopy, using pseudogrisms H and K (Fragoso-López et al. 2008).

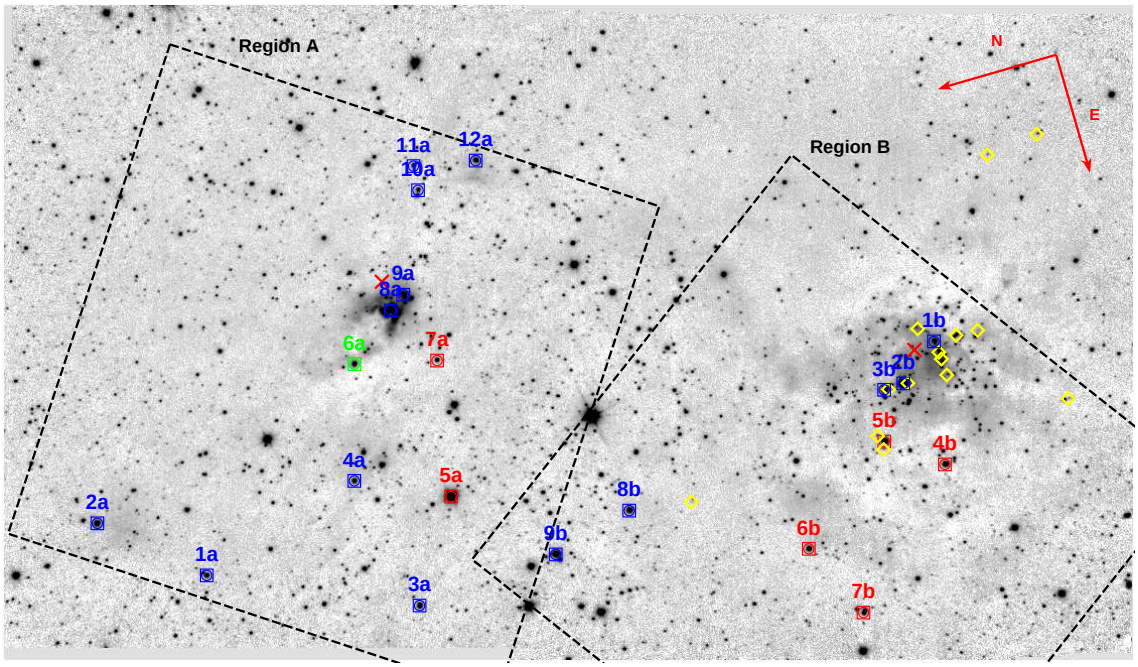

Fig. 2. Masgomas-4 K_S image obtained with LIRIS. Stars with spectral classification are marked with blue (OB-type dwarfs), green (A, F, and G dwarfs), and red squares (giant stars). We also mark with yellow rhombi the Herbig Ae/Be candidates and with red crosses the position of the IRAS sources. Orientation is the same as in Figure 1 to help comparison between the figures. Length of orientation arrows is 1 arcmin, and black squares show the orientation of both multi-object masks (regions A and B).

The candidate apparent size is larger than the LIRIS field of view. Therefore, we divide it into two regions. Region A, centred around α_{2000} = 18^{h}56^{m}05.95^s, δ_{2000} = +07°56′52.6″ and including the IRAS source IRAS 18536+0753, and region B, centred on α_{2000} = 18^{h}56^{m}11.09^s, δ_{2000} = +07°53′06.5″ and containing the IRAS source IRAS 18536+0749. The angular distance between both centres is 4′16″.

We obtained the cluster and control field images on 2010 June 23, with seeing values between 0.70 – 0.80″ (see Table 1). We observed using a nine-point dithering mode to improve cosmic-ray reduction and bad-pixel reduction, and to construct the sky image for subtraction at a later time. For image reduction (bad-pixel mask, flat correction, sky subtraction, and alignment), we followed a similar procedure to the one described by Ramírez Alegría et al. (2012). Data reduction was made with FATBOY (Eikenberry et al. 2006) and the LIRIS reduction package LIRISDR[2]. The final K_S image shown in Figure 2 is a composite of regions A and B individual images.

Instrumental photometry was made with DAOPHOT II, ALLSTAR, and ALLFRAME (Stetson 1994). It was cleaned of non-stellar and poorly measured objects using the sharp index (-0.25 < sharp < 0.25) and PSF fitting σ < 0.1. For photometric calibration, we used 37 stars from region A and 48 stars from region B. These stars, part of the 2MASS catalogue (Skrutskie et al. 2006), are isolated and non-saturated stars in our photometry. For stars brighter than J < 14 mag, H < 11.5 mag, or K_S < 9.5 mag, we assumed the magnitudes from the 2MASS catalogue.

For our data we define the limiting magnitude as the characteristic magnitude with a photometric error of 0.21 mag. This photometric error limit corresponds to a signal-to-noise ratio of 5 (Newberry 1991). In Figure 3, we show the K_S magnitude and its associated error for the Masgomas-4 photometry, and the exponential function fitted to the data. Using this function we estimated that the limiting magnitude for the K_S band is 16.7 mag.

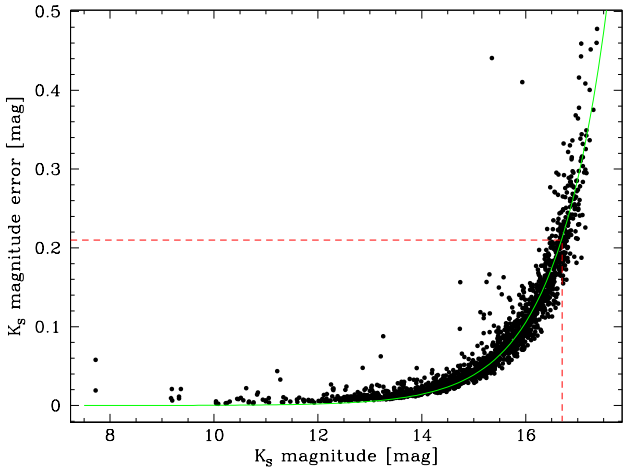

Fig. 3. Calibrated K_S magnitude versus photometric error for Masgomas-4. We show with a green solid line the exponential function fitted to the data, and with a red segmented line the limiting magnitude of K_S ~16.7 mag associated with the photometric error of 0.21 mag (or a signal-to-noise ratio of 5).

We used SKYCAT for the astrometric calibration, by correlating image and equatorial coordinates for the same set of stars used in the photometric calibration. Fitting errors are less than 0.15 arcsec for the three filters.

Near-infrared spectra were observed during 2011 September 14, 15, and 16 (half nights, Table 1). As shown in next section, two masks were designed to observe the OB-type star candidates. We included in the region A mask (hereafter mask A) twelve stars, and in the region B mask (mask B), nine stars. To

[2] http://www.iac.es/project/LIRIS

Table 1. Summary of imaging and spectroscopic observations

Observing mode	Date	Filter	Exp. time [s]	Seeing [″]	Airmass
Masgomas-4 field imaging	2010 June 23	J	108.0	0.78	1.17–1.21
(A, B, and control)	2010 June 23	H	79.2	0.72	1.22–1.27
	2010 June 23	K_S	79.2	0.70	1.28–1.36
MOS (R∼2500)	2011 September 16	H	2520.0	0.83	1.18–1.35
Mask region A	2011 September 16	K	1920.0	0.86	1.40–1.63
MOS (R∼2500)	2011 September 14	H	1800.0	0.78	1.47–1.75
Mask region B	2011 September 14	K	2880.0	1.59	1.07–1.10
Telluric standard (R∼2500)	2011 Sept 14	H	1080.0	0.95	1.59–1.94
	2011 Sept 14	K	1800.0	1.12	1.07–1.19
	2011 Sept 16	H	1040.0	1.16	1.50–1.88
	2011 Sept 16	K	960.0	1.63	1.94–2.56

avoid large signal-to-noise differences for spectra with the same exposure times, we limited the magnitude difference in each mask to less than 2 mag (for K_S). Slits of 0.8 arcsec in width and 8-10 arcsec in length were cut on each mask, which produced a resolution of R 2500. The typical values for the signal-to-noise is ∼ 76.7 for H band spectra, and ∼ 78.6 for K band spectra, per resolution element. We also took into account the slit position along the dispersion axis, a key factor to obtain the right wavelength range to observe OB-type characteristic spectral lines. The telluric standard for all spectra was the A0 V star HD 231033, and the modelling of the A0 V spectral contribution was carried out with XTELLCOR (Vacca et al. 2003). The subtraction of the telluric lines and the correction due to the airmass difference were completed with the IRAF task TELLURIC.

3. Results

In the first part of this section we show the photometric diagrams (colour–magnitude, colour–colour, and pseudocolour–magnitude) for regions A, B, and the control field. The second part of the section is dedicated to the infrared spectra from Masgomas-4, and the description of the spectral features used for the spectral classification.

3.1. Photometry

In the colour–magnitude diagrams (CMD) for regions A and B (Figure 4) the cluster main sequence is not clearly seen. Differential extinction spread it to redder colours, following the reddening vector. This makes it difficult to distinguish the cluster stars among the field stars using only the CMD. It is therefore necessary to use extra photometric colours to clearly spot the cluster stellar population. For this purpose we used the reddening-free parameter Q_{IR} (Comerón & Pasquali 2005; Negueruela & Schurch 2007) to identify the OB-type star candidates in regions A and B.

The definition of the parameter Q_{IR} depends on the assumed extinction law, which can be determined from the regions' colour–colour diagrams (CCD, Figure 5). These diagrams show that the extinction in regions A and B is accurately described by the Rieke extinction law (Rieke et al. 1989), with $R = 3.09$ (Rieke & Lebofsky 1985).

The slopes of the linear function fitted to the $(H-K_S)$-$(J-H)$ diagrams are

$$\frac{\mathrm{E(J-H)}}{\mathrm{E(H-K_S)}} = 1.69 \pm 0.03 \quad (1)$$

for region A and

$$\frac{\mathrm{E(J-H)}}{\mathrm{E(H-K_S)}} = 1.66 \pm 0.04 \quad (2)$$

for region B. These values are in agreement, within errors, with the value derived from the Rieke extinction law:

$$\frac{\mathrm{E(J-H)}}{\mathrm{E(H-K_S)}} = 1.70. \quad (3)$$

Using the reddening-free parameter Q_{IR} defined by this extinction law

$$Q_{IR} = (J-H) - 1.7 \cdot (H-K_S), \quad (4)$$

we can see in both pseudocolour–magnitude diagrams a vertical sequence around $Q_{IR} \sim 0$ mag (Figure 6). These sequences, which are understood as OB-type star candidates, are not seen in the control field's pseudocolour–magnitude diagram. Therefore, it is a feature associated with the cluster stellar population.

In the colour–magnitude diagrams we can also see a group of bright and reddened stars, close to $K_S \sim 10$ mag and $(J-K_S) \sim 4$ mag. These stars could be part of the upper end of the cluster main sequence, spread by the differential extinction to dimmer magnitudes and redder colours. Because these objects have pseudocolour values of $Q_{IR} \sim 0.6$ mag, they are most probably giant stars from the galactic disc.

For multi-object spectroscopy we selected stars with reddening-free parameter Q_{IR} between −0.2 mag and 0.2 mag. We also selected some stars, outside this Q_{IR} range, due to their position in the Masgomas-4 field (see Fig. 2). For example, star 7a ($Q_{IR} = 0.50$ mag) is located at the centre of region A; star 8a has $Q_{IR} = -0.52$ mag and is also a central star in region A; star 6b ($Q_{IR} = 0.84$ mag) is located on the edge of a bubble-shaped structure in region B; star 11a has a value of $Q_{IR} = 0.25$ mag and, because it does not overlap with any other slit in the mask, we decided to include it.

A second group of stars are blue objects with an interesting position in the cluster field. For example star 6a, which is

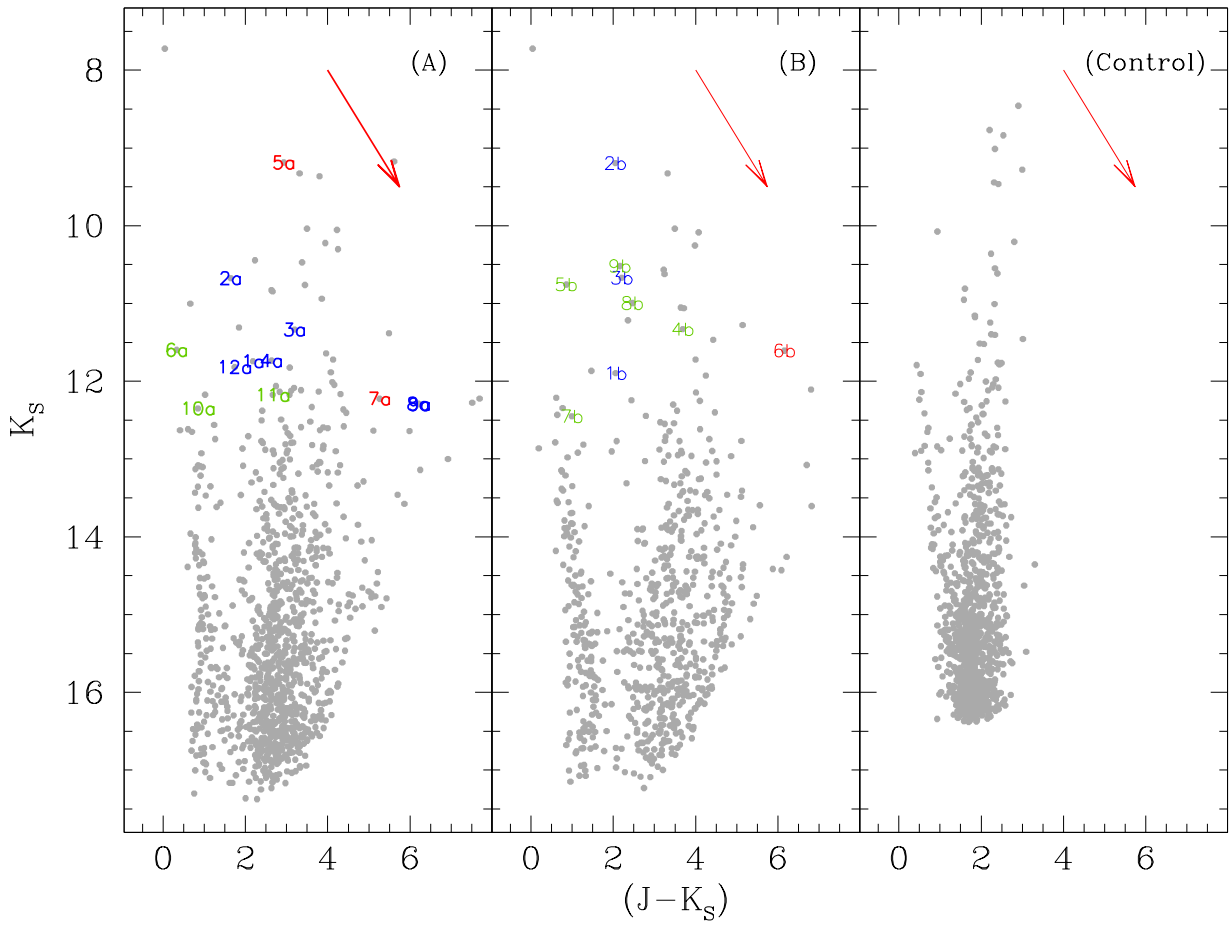

Fig. 4. Cluster colour–magnitude diagrams (CMD) for regions A (left), B (middle), and the control field (right). We label the spectroscopically observed and classified stars using their numbering for masks A and B. We indicate the OB-type stars with blue symbols; A-, F-, and G-type dwarfs with green symbols; and giant stars with red symbols. The red arrow shows an extinction of A_{K_S} =1.5 mag, assuming the extinction law from Rieke et al. (1989), with R = 3.09 (Rieke & Lebofsky 1985).

located in one arm-shaped structure of IRAS 18536+0753, and star 5b, which is close to the bubble-shaped structure of IRAS 18537+0749.

Finally we identify a group of very reddened stars in the region B CCD. This could indicate the existence of a younger (and more embedded) population in region B. These objects are shown with yellow rhombi in Figure 2.

3.2. Spectral classification

Spectral classification for Masgomas-4 has followed a similar procedure to that in previous group works (G61.48+0.09 Marín-Franch et al. 2009; Sh2-152, NGC 7538 Puga et al. 2010; Ramírez Alegría et al. 2011; and Masgomas-1, Ramírez Alegría et al. 2012). The classification scheme is based on the detection of absorption lines and the comparison of their depth and shape with similar resolution spectra of known spectral types. The catalogues used for spectral classification were Hanson et al. (1996) (K band) and Hanson et al. (1998) (H band), for OB-type stars, and Meyer et al. (1998); Wallace & Hinkle (1997) for late-type stars. For the assigned spectral type we assume an error of ±2 subtypes, similar to Hanson et al. (2010), Negueruela et al. (2010), and Ramírez Alegría et al. (2012).

Table 2 provides the coordinates, infrared magnitudes, and spectral types of the spectroscopically observed stars. The mask A and mask B final spectra, as well as the telluric correction spectra, are shown in Figures 7 (OB-type stars) and 8 (AFG-type dwarfs and giants stars).

According to the stellar spectra, we can separate the observed stars in three groups: OB-type stars, AFG-type dwarfs, and giant stars.

3.2.1. OB-type stars

These stars are identified by their helium lines and incomplete Brackett series. According to the observed spectral features, star 2b is the earliest object in our set. The spectrum has strong He I lines at 1.70 and 2.11 μm, similar to those found in O9.5 V stars (for example, HD 37468 or HD 149757, Hanson et al. 2005) and Brackett series similar to an O9 V star (v.g. HD 193322, Hanson et al. 1996). We have adopted a spectral type O9–9.5 V for this star.

Star 3b shows features of a slightly later star. The Brackett series is deeper and similar to the B2 V HD 36166 star (Hanson et al. 2005), and its clear He I lines are similar to the B0 V HD 36512 star (Hanson et al. 1996). We classify star 3b as B1 V.

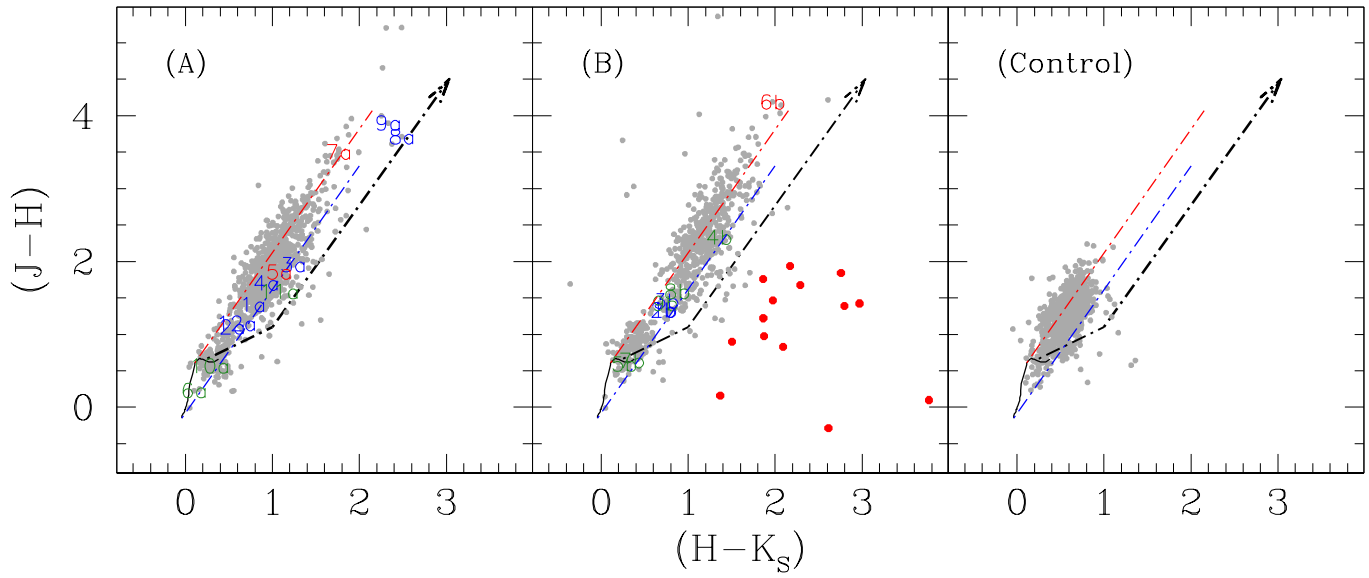

Fig. 5. Cluster CCDs for regions A (left), B (middle), and the control field (right). We use the same symbols as in Figure 4 to mark the spectroscopically observed stars. In the diagrams we mark with segmented lines the position of an O8 V (blue lines) and a K5 V star (red lines), following the Rieke extinction law (Rieke et al. 1989), as used in this work. Thicker black segmented lines show the expected position for T Tauri stars along the extinction vector. In the region B diagram, we show with red circles the stars with infrared excess, candidates to Herbig Ae/Be objects.

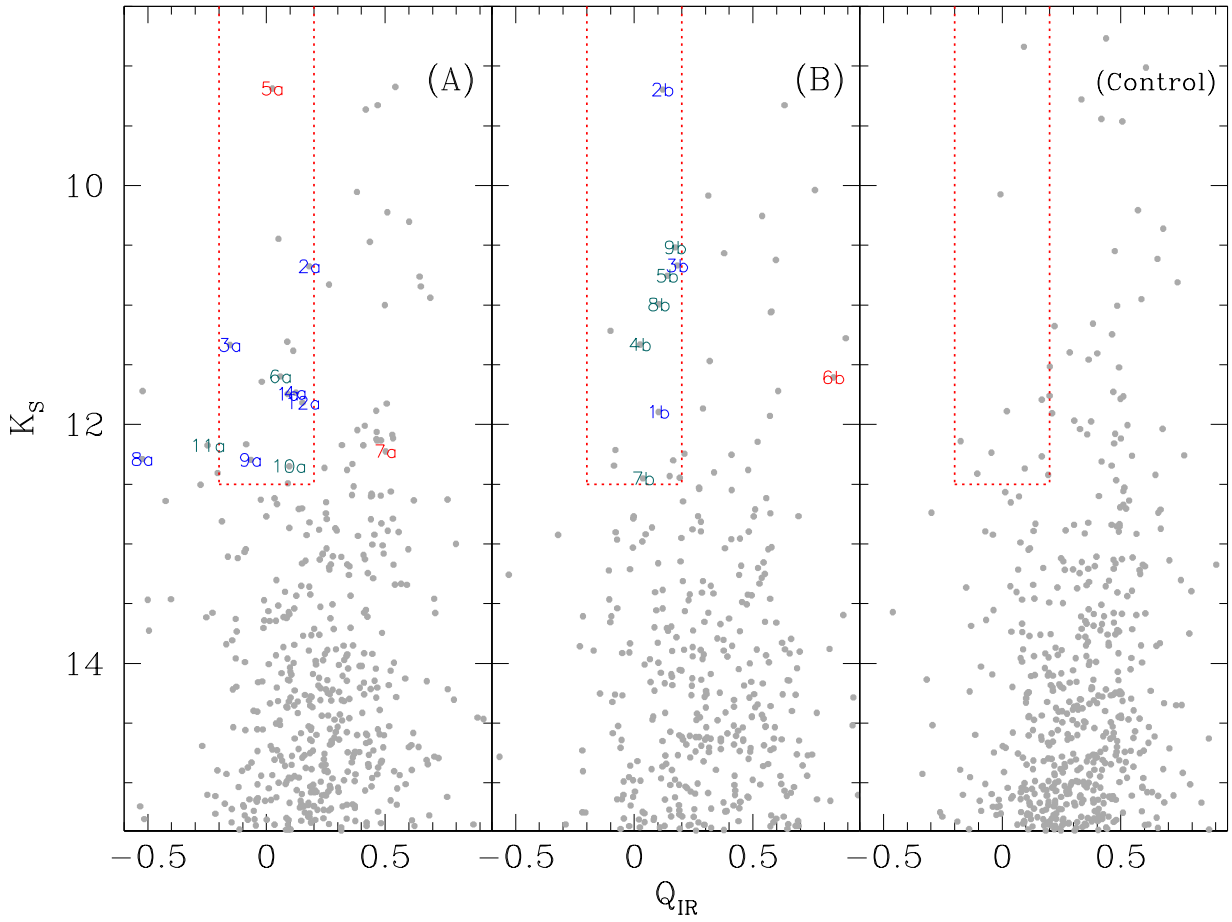

Fig. 6. Cluster pseudocolour–magnitude diagrams for regions A (left), B (middle), and the control field (right). We use the same symbols as in Figure 4 to mark the spectroscopically observed stars (blue=OB-type, green=A-, F-, G-type, red=giants). Dotted red lines mark the adopted limits in pseudocolour Q_{IR} and magnitude K_S for the OB-candidates selection.

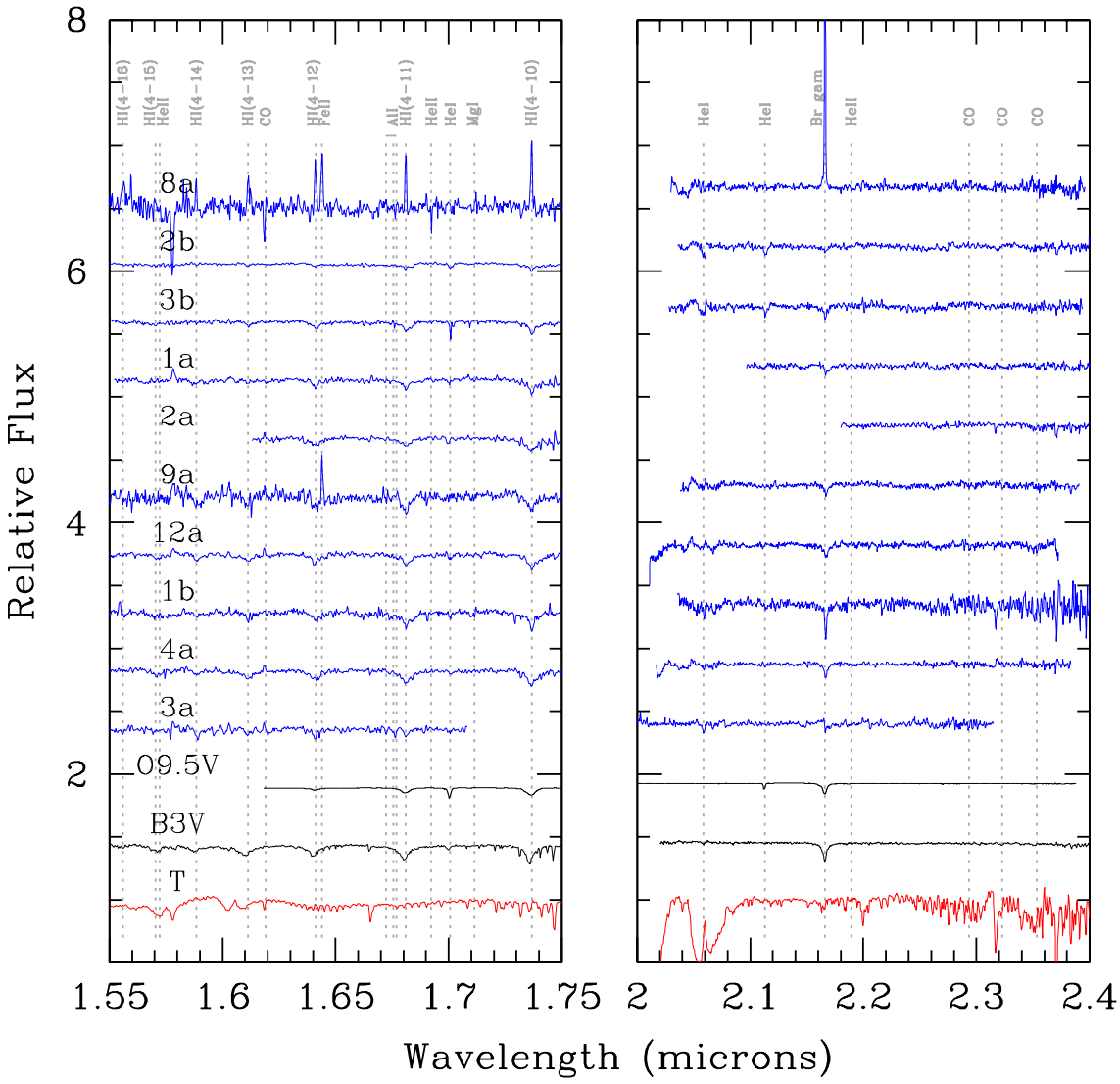

Fig. 7. Individual spectra in *H* (left) and *K* band (right) for OB-type stars. Spectral features used in the spectral classification are labelled in grey. We show in black two spectra from the spectral libraries for comparison: O9.5 V HD 37468 (Hanson et al. 2005, degraded to our resolution) and B3 V HR5191 (Meyer et al. 1998). The telluric correction spectrum is shown in red.

Spectra of stars 1a, 2a, and 9a show weak Brackett series, until H I (4-12), with a depth similar to a B3 V star (v.g. HR 5191, Meyer et al. 1998). The weak He I line at 1.70 μm indicates a stellar type similar to a B2 V star, so we adopt a spectral type B2–3 V for these stars. The spectrum of star 1a shows an emission at 1.58 μm and others stars (v.g. stars 3a, 6a, 9a, 10a, 11a, and 12a) show an emission bump at this position. Inspecting the telluric correction spectrum, we see an absorption at the same position. We understand it to be an artifact from the reduction process and not a real stellar line. The Brackett series for star 2a is wider than the other star series, indicating that star 2a could be a fast rotator.

In the case of spectrum 9a, we also see an emission feature close to the H I (4-12) line, also seen in the 8a spectrum, that can be identified as an Fe II line. This line indicates the presence of circumstellar material, and can be found in Herbig Be stars (Puga et al. 2010). Because for star 9a we observe its Brackett series in absorption, we understand that this object is as very young, but already in the main sequence.

In the spectra of stars 12a and 1b we observe an *H* band spectrum similar to a B3 V star (Meyer et al. 1998), with a Brackett series extending until HI (4-15), and a clear He I at 1.70 μm. The *H* band spectrum indicates a B3 V spectral type for both stars.

The Brackett series for spectrum 4a extends until H I (4-15) line and looks similar to that observed in B3 V stars (Meyer et al. 1998; Ranade et al. 2004). Around 1.70 μm we find a weak feature, that could be a He I line, and the *K* band spectrum is similar to the one observed in B3-5 V type stars (Hanson et al. 1996, 1998), which we adopt as spectral type for 4a.

Finally there are two stars in this group without a clear spectral classification. The first one is star 3a, with an irregular Brackett series and an asymmetric Brγ line. We see the He I lines at 1.70 μm and at 2.06 μm, but the last one is located at a wavelength with a problematic telluric correction. Because this spectrum is noisy and most of its Brackett series is within the noise level, we cannot clearly classify it. Both the presence of He I at 1.70 μm and the absence of He II limit the star 3a spectral type to early B-type.

The second star, 8a, presents the Brackett series in strong emission for both *H* and *K* bands. No extended emission was detected during the reduction process, indicating that the emission comes from the immediate vicinity of the star. Its spectrum

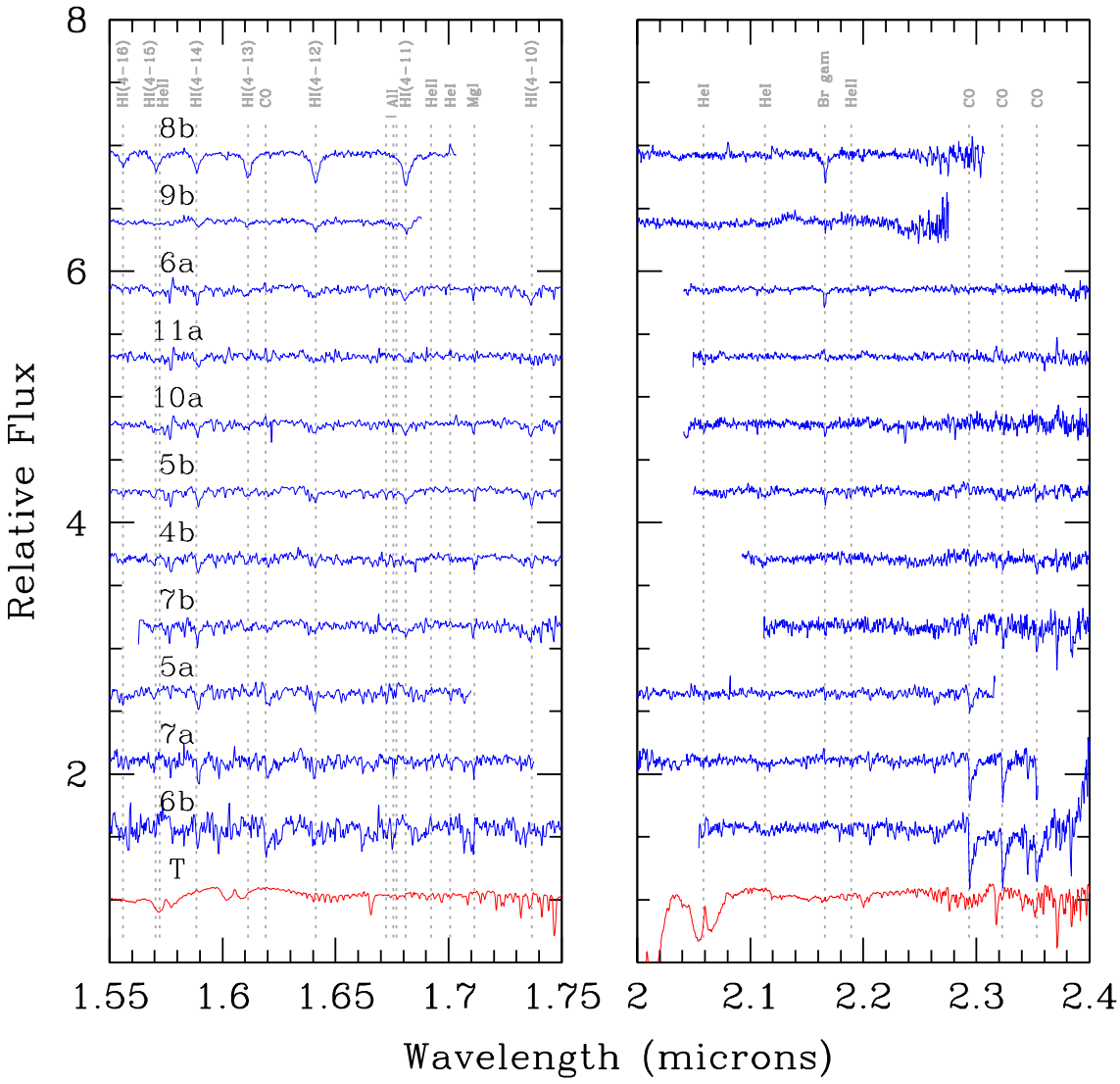

Fig. 8. Individual spectra in *H* (left) and *K* band (right) for the AFG-type dwarfs and the giant stars. We show in grey the spectral lines used for the spectral classification. The red spectrum corresponds to the telluric correction spectrum, shown for spectral feature comparison.

shows FeII at 1.64 μm in emission, which indicates that it is very young, probably still surrounded by circumstellar material, as described by Puga et al. (2010) for their star 26. Because of the complete emission Brackett series, the emission Fe II line at 1.64 μm and the colours of this star, we classify it as a young stellar object (YSO).

3.2.2. A-, F-, and G-type dwarfs

The observation of this type of stars was expected as contamination, because the pseudocolour Q_{IR} for OB and AF-type dwarfs is similar. The earliest star in this group, 8b, only presents in its spectrum a clear Brackett series, extended until the H I (4-18) line. No metallic lines are clearly distinguished in this spectrum, and we assign it the A5 III-V spectral type.

For F-type stars, the Brackett series begins to diminish, and Mg I lines at 1.57, 1.71, and 2.2 μm become stronger. In the star 9b spectrum the H I (4-11), (4-12), and (4-13) lines are present and similar to those observed in F3 V (Meyer et al. 1998) or F7 V stars (Meyer et al. 1998). Even if Mg I is not clearly seen in the star 9b spectrum, we assign the F3-7 V spectral type .

For stars 6a (F6 V), 11a (F6-8 V), and 10a (F8 V), the Brackett series does not extend beyond the H I (4-13) line, their Brγ lines are narrow and deep, and the Mg I lines in the *H* band spectrum are similar to those seen in late F V stars (Meyer et al. 1998).

The spectrum of star 5b presents late F-type features and a faint ^{12}CO (2,0) band. The presence of this band indicates an early G-type for this star. The *H* band spectrum is similar to an F6 V star (Meyer et al. 1998), but the *K* band spectrum is more similar to an F8.5 V star, considering the Brγ line's depth and the Mg I line at 2.28 μm (Meyer et al. 1998). Because of the faint presence of the CO band, we assign this star a spectral type between F6 and G1 V.

The spectrum of star 4b presents clear Mg I lines in *H* and *K* bands; its Mg I lines at 1.57 and 1.71 μm are broad but not as deep as expected for a G2 V star. The *K* band spectrum does not show the Brγ line, discarding a luminosity class III for this object, and its ^{12}CO (2,0) band fit the band from a G2-3 V star.

In the case of the star 7b, we observe that the Mg I lines are similar in depth and shape, to a G8 V or K0 V star. The *K* band spectrum shows a shallow ^{12}CO (2,0) band and a deep Ca I line

Table 2. Stars with observed spectra. We include the equatorial coordinates, infrared magnitudes (J, H, K_S), and spectral type for each star. For those stars with estimated luminosity class, we have included the extinction and distance estimates.

ID	RA (J2000) [h m s]	dec (J2000) [° ′ ″]	J [mag]	H [mag]	K_S [mag]	Spectral type	A_K [mag]	Distance [kpc]
OB-type dwarfs:								
2b	18 56 11.98	+07 53 38.1	11.246 ± 0.008	9.911 ± 0.008	9.196 ± 0.006	O9–9.5 V	$1.47^{+0.02}_{-0.03}$	$1.77^{+0.26}_{-0.67}$
3b	18 56 11.99	+07 53 48.1	12.875 ± 0.003	11.419 ± 0.004	10.767 ± 0.004	B1 V	$1.54^{+0.03}_{-0.02}$	$2.08^{+1.43}_{-0.99}$
1a	18 56 11.05	+07 59 31.0	13.926 ± 0.014	12.519 ± 0.010	11.744 ± 0.006	B2–3 V	$1.52^{+0.03}_{-0.02}$	$2.47^{+2.24}_{-0.77}$
2a	18 56 08.31	+08 00 14.3	12.318 ± 0.018	11.217 ± 0.002	10.676 ± 0.005	B2–3 V	1.16±0.01	$1.52^{+0.95}_{-0.29}$
9a	18 56 04.21	+07 57 17.9	18.526 ± 0.014	14.628 ± 0.046	12.296 ± 0.020	B2–3 V	$4.19^{+0.03}_{-0.02}$	$0.93^{+0.84}_{-0.29}$
12a	18 56 00.73	+07 56 24.3	13.554 ± 0.028	12.404 ± 0.005	11.818 ± 0.007	B3 V	1.21±0.02	$2.13^{+1.93}_{-0.22}$
1b	18 56 10.97	+07 53 17.6	13.954 ± 0.005	12.620 ± 0.005	11.895 ± 0.006	B3 V	1.43±0.02	$2.00^{+1.81}_{-0.21}$
4a	18 56 09.55	+07 58 08.3	14.370 ± 0.007	12.665 ± 0.007	11.734 ± 0.005	B3–5 V	1.80±0.02	$1.48^{+0.67}_{-0.22}$
3a	18 56 14.12	+07 57 56.5	14.530 ± 0.007	12.575 ± 0.004	11.335 ± 0.011	B0–5 V	2.19±0.03	$1.68^{+1.19}_{-0.70}$
8a	18 56 04.57	+07 57 26.1	18.489 ± 0.092	14.779 ± 0.033	12.289 ± 0.021	YSO	–	–
A, F, G dwarfs:								
8b	18 56 13.22	+07 56 04.6	13.459 ± 0.003	11.847 ± 0.003	11.100 ± 0.005	A5 III–V	$1.58^{+0.02}_{-0.03}$	$0.38^{+0.04}_{-0.03}$
9b	18 56 13.86	+07 57 45.3	12.678 ± 0.005	11.254 ± 0.005	10.615 ± 0.010	F3–7 V	$1.25^{+0.03}_{-0.02}$	0.21±0.00
6a	18 56 05.90	+07 57 50.9	11.926 ± 0.021	11.697 ± 0.004	11.597 ± 0.008	F6 V	$0.04^{+0.03}_{-0.02}$	0.61±0.01
11a	18 56 00.29	+07 56 53.9	14.839 ± 0.009	13.253 ± 0.008	12.175 ± 0.006	F6–8 V	1.56±0.02	0.40±0.04
10a	18 56 01.09	+07 56 55.4	13.195 ± 0.031	12.627 ± 0.006	12.349 ± 0.008	F7 V	0.36±0.02	$0.74^{+0.08}_{-0.07}$
5b	18 56 13.62	+07 53 55.6	11.613 ± 0.002	11.022 ± 0.002	10.810 ± 0.027	F6–G1 V	0.35±0.02	$0.33^{+0.05}_{-0.04}$
4b	18 56 14.93	+07 53 30.7	14.950 ± 0.005	12.661 ± 0.006	11.483 ± 0.004	G2–3 V	$2.19^{+0.01}_{-0.02}$	$0.15^{+0.16}_{-0.01}$
7b	18 56 18.78	+07 54 30.9	13.445 ± 0.005	12.788 ± 0.011	12.508 ± 0.009	G8–K0 V	$0.25^{+0.03}_{-0.05}$	$5.44^{-0.54}_{+1.30}$
Giant stars:								
5a	18 56 11.00	+07 57 25.6	12.121 ± 0.018	10.265 ± 0.013	9.188 ± 0.021	G4–7 III	1.58±0.02	$0.57^{-0.03}_{+0.04}$
7a	18 56 06.61	+07 57 12.0	17.490 ± 0.036	13.989 ± 0.010	12.225 ± 0.005	K0–2 III	$3.02^{+0.05}_{-0.08}$	$1.67^{-0.32}_{+0.83}$
6b	18 56 16.22	+07 54 46.8	17.764 ± 0.051	13.576 ± 0.010	11.606 ± 0.004	M0–1 III	$3.39^{+0.01}_{-0.05}$	$3.11^{-0.27}_{+1.18}$

at 2.27 μm. Even if the deep of the CO band is similar to the K0 V or K5 V CO band, the depth of the Ca I line indicates an earlier spectral type for this object, between G8 and K0 V.

3.2.3. Giant stars

The three stars from this group present late-type spectral lines that allow us to classify them as luminosity class III. The spectra of stars 5a, 7a, and 6b have clear ^{12}CO (3,0) bands in H, characteristic of luminosity classes I or III, and not observed in stars with luminosity class V. The equivalent widths for the ^{12}CO (2,0) band in K, between 2.294 μm and 2.304 μm, are EW_{6b} = 17.60 Å, EW_{5a} = 4.23Å, and EW_{7a} = 8.96Å; these values fit better a luminosity class III for the three stars, according to the equivalent width and luminosity class relation given by Davies et al. (2007), and the spectral type adopted for these three stars.

The star 5a spectrum is similar to a G4III or a G7III spectra (Wallace & Hinkle 1997) in the K band. In the H band it is similar to a G6 III (Meyer et al. 1998). We adopt the spectral type G4–7 III for this star.

The CO depth in H for star 7a is similar to that observed in the HR 7949 spectrum (spectral type K0 III, Meyer et al. 1998), and the CO band in K fits the HR 8694 (spectral type K0 III, Wallace & Hinkle 1997) or the HR 6299 band (spectral type K2 III, Wallace & Hinkle 1997). For this star we adopt a spectral type K0–2 III.

Finally, for the star 6b we have adopted a M0–1 III spectral type, based on its K band spectrum, which is similar to the HR 4069 and the HR 7635 spectra (spectral types M0 III, Wallace & Hinkle 1997), and its H band spectrum, similar to the HR 4517 spectrum (spectral type M1 III, Meyer et al. 1998).

4. Discussion

4.1. Distance estimate

From the stars observed spectroscopically, 19 out of 21 were selected following the pseudocolour Q_{IR} criteria (including star 11a, which has Q_{IR} = 0.25, slightly beyond the upper limit). The other two (i.e. 7a and 6b) were chosen because of their field position. From the 19 stars, 10 were classified as OB-type dwarfs.

For all the stars but one (i.e. star 8a), we derive individual distances by comparing apparent and intrinsic magnitudes according to the assigned spectral type. We assume visual magnitudes from Cox (2000), intrinsic infrared colours from Tokunaga (2000), and the extinction law from Rieke et al. (1989) with R = 3.09 (Rieke & Lebofsky 1985). The choice of this extinction law was justified in Section 3.1. The K_S-filter extinction, expressed as

$$A_{K_S} = \frac{E_{J-K_S}}{1.514} \quad (5)$$

varies between 0.04 mag and 4.19 mag, equivalent to A_V between 0.37 mag and 38.66 mag.

Distance errors were dominated by the spectral type uncertainties, which we estimate by deriving the individual distance for the same star assuming ±2 spectral subtypes. The distance errors associated with photometric errors were generally less than 10% of those derived from the spectral type uncertainty and therefore were not included in the error estimates. For stars with a range in spectral type (for example star 1a, B2–3 V), we assume the individual distance estimate to be the mean between the distance associated with each spectral type defining the range.

In Table 2 we present the individual extinction and distance determination for the OB-type stars used in the cluster distance estimate. These estimates are also shown in Figure 9, where we

present regions A (red) and B (blue) individual distances and extinctions for OB (left) and non-OB (right) type stars. In the figure we show the mean distance value for regions A (three-pointed star) and B (four-pointed star), and we can observe that:

- In region A, OB-type stars have a mean distance of $1.87^{+1.29}_{-0.77}$ kpc. For this determination, we have excluded stars 8a and 9a, both belonging to the nucleus of region A. Because star 8a has not been spectroscopically classified, the extinction and distance could not be estimated for this object. For star 9a, the spectroscopically observed star with the largest reddening, photometry is probably contaminated by local nebulosity, making the measured magnitude unreliable.
  Even without an extinction or distance estimate for stars 8a and 9a, their positions in the CCDs indicate that these stars are not foreground objects.
- In region B, a mean distance of $1.95^{+1.21}_{-0.76}$ kpc was derived from stars 1b, 2b, and, 3b individual distances. This distance is in agreement within errors with the one derived for IRAS 18537+0753: 2.1 kpc (Plume et al. 1992), and the estimate derived from the observations of the methanol maser [HHG86] 185345.9+074916: 2.2 kpc (Val'tts et al. 2000).
  We conclude that stars 1b, 2b, and 3b are associated with the IRAS source IRAS 18537+0753, the methanol maser, and the massive star forming region Sh2-76 E.
- Dwarfs stars with spectral type A, F, or G have individual distances less than 1 kpc. Consequently we classify these objects as foreground dwarf stars from the galactic disc.
  The exception in this group is star 7b, with a distance estimate of d = 5.44 kpc. After reviewing the LIRIS images we notice that this star is contaminated by a close companion, and their radial profiles are merged. Because of this contamination, we exclude the star 7b from the analysis.
- Giant stars have two types of extinction and distance values: the foreground star 5a, probably located in the same structure as A-, F-, and G-type stars; and the background giant stars 5a and 6b. In both cases these stars are part of the giant population of the galactic disc.

The OB-type stars from the cores in regions A and B are located at the same distance within errors. We thus conclude that they belong to two near-infrared nuclei of a single, young, massive, and embedded stellar population. Using the mean distance of regions A and B, we estimate a distance of $1.90^{+1.28}_{-0.90}$ kpc for the Masgomas-4 association, with a mean extinction A_K=1.54±0.02 mag. At this distance, the projected separation of regions A and B corresponds to a linear separation of about 2.4 pc.

In the CCDs (Fig. 5) we observe objects in the T Tauri region, below the black segmented line. The T Tauri candidates are present in both regions A and B, but only in the case of region B we identify a group of objects with extra reddening (colours $(H - K_S) > 2$, shown with red circles in the CCD of region B). These stars (or protostars) are concentrated around the region B nucleus, as can be seen in Figure 2, and their extra reddening can be explained by the presence of circumstellar accretion discs.

Because of the extra reddening of this group of stars, compared with the colours of the T Tauri objects, we classify them as Herbig Ae/Be candidates. According to Subramaniam et al. (2006), Herbig Ae/Be objects are located to the right of the locus of the classic T Tauri objects in the CCDs. These objects are also younger, more embedded, and more massive than T Tauri objects.

Like Masgomas-1 (Ramírez Alegría et al. 2012), Masgomas-4 is located in the direction of the RSG clusters. Our distance estimate discards a physical link of Masgomas-4 with the intersection between the close end of the Galactic bar and the Scutum-Centaurus arm base. The 1.90 kpc distance estimate places Masgomas-4 closer than the Scutum-Centaurus arm, probably in the Carina-Sagittarius arm.

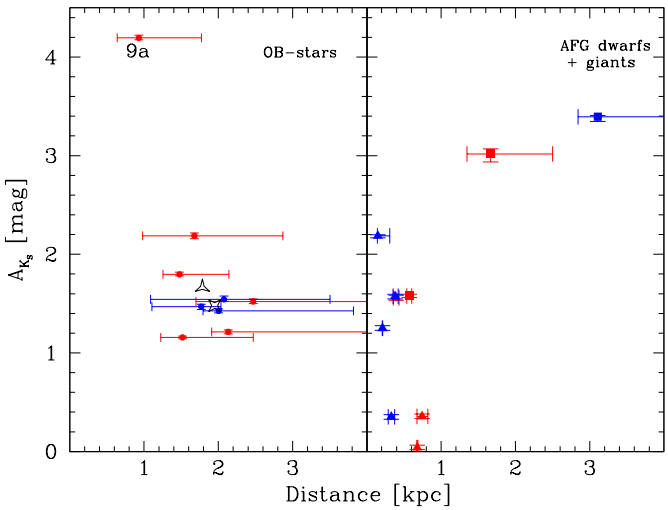

Fig. 9. *Left:* Individual distances and extinctions for OB-type stars. Red symbols show the parameters for region A stars, and blue symbols for region B stars. Mean values of distance and extinction for regions A and B stars are marked with three- and four-pointed black stars, respectively. *Right:* Individual distances and extinctions for non-OB stars in regions A (red symbols) and B (blue symbols). Estimates for spectral type A, F, and G dwarfs are shown with triangles, and giant stars estimates are shown with squares.

4.2. Mass and age estimates

To estimate the cluster's present-day total mass, we follow a similar procedure to that described by Ramírez Alegría et al. (2012). We fit a Kroupa (Kroupa 2001) initial mass function (IMF) to the cluster present-day mass function, and integrate it from log $(M) = -1.0$ dex to 1.5 dex. Because there is not an evolved stellar population in Masgomas-4, we can assume that the difference between the initial and present mass function in the cluster is small.

We fit the Kroupa IMF to the cluster mass function between ~2.5 $M_\odot$ and ~35 $M_\odot$. The mass function was derived from the luminosity function and the contribution from the galactic disc stellar population was corrected using the observed control field (from LIRIS images). The cluster and control field photometries were cut in $J < 16.5$ mag, $H < 15.5$ mag, and $K < 14.5$ mag, to assure a completeness close to 1.0, following the same procedure described by Ramírez Alegría et al. (2012).

To obtain the luminosity and mass functions, we project every star, following the reddening vector, to the main sequence located at 1.9 kpc. This sequence is defined by the colours and magnitudes given by Cox (2000), and is expressed analytically by two lines: one from the spectral type O9 V to A0 V, and the second one from A0 V to G0 V, corresponding to the last spectral type to the limit magnitude chosen for completeness.

To derive the mass function we convert the K_S magnitudes to solar masses, using the values given by Cox (2000) for stars later than B0 V, and Martins et al. (2005) for stars earlier than

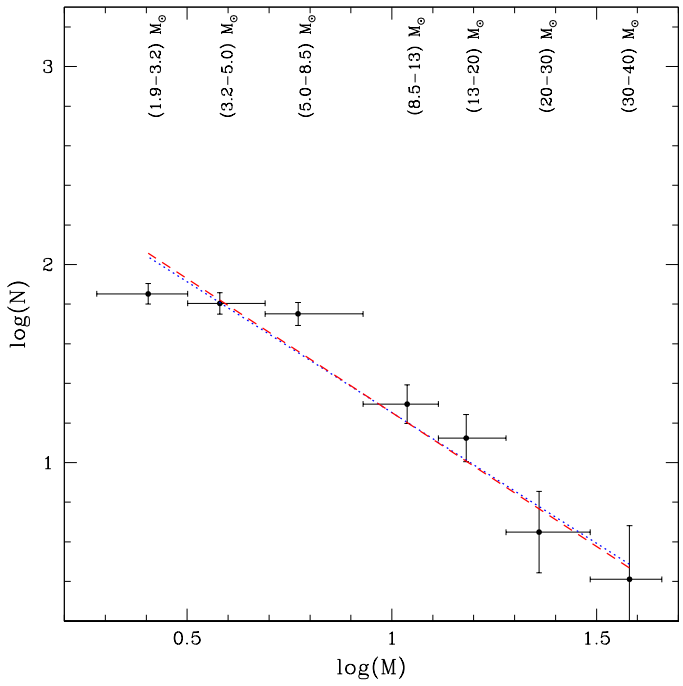

Fig. 10. Present-day mass function for Masgomas-4. Points show the central position in the mass ranges indicated above them, and the segmented red line corresponds to the Kroupa IMF fitted to the data. As a comparison, we show the least-squares fitting (one degree function) to our data with a blue dotted line.

this. For magnitudes that were between values in the catalogue, we interpolate between the two closest values.

After subtracting the Masgomas-4 field and the control field mass function, we obtain the cluster present-day mass function, shown in Figure 10. We fit a Kroupa IMF and integrate in the mass range 0.10-31 $M_{\odot}$ (equivalent to log $(M) = -1.0$ dex to 1.5 dex), estimating a total cluster mass (lower limit) of $(2.19 \pm 0.31) \cdot 10^3 M_{\odot}$. The Kroupa IMF fitting is also compared in the figure with a least-squares fitting to the data. Both fits are similar within data errors.

Cluster age can be limited by the presence of an O9 V star. This gives an upper limit of 10 Myr that could be reduced by the confirmation of earlier stars in the centre of region A, for example star 8a. This age limit of 10 Myr is also dependent on the rotation speed assumed by the stellar evolutionary models (Brott et al. 2011).

The presence of T Tauri and Herbig Ae/Be candidates also gives information about the cluster age. According to Hernández et al. (2007) in young clusters (age $\sim$ 3 Myr), 30% of the T Tauri objects and 15% of the Herbig Ae/Be objects lose their circumstellar discs. The survivor discs around Herbig Ae/Be objects will be lost in less than 10 Myr.

Although there is a difference because of the presence of Herbig Ae/Be candidates in region B, which are absent in region A, both cores display signs of on-going star formation (IRAS sources and masers). The presence of Herbig Ae/Be candidates also limits the age of the recent burst in the region B core to 5 Myr.

Lada & Lada (2003) indicate that it is very unlikely to find embedded clusters older than 5 Myr. Because part of the stellar population of Masgomas-4 is still deeply embedded and the whole cluster is surrounded by an H II cloud, we adopt this value as a new upper limit for the cluster age, limiting the cluster age to 5 Myr.

5. Conclusions

We present the observations, physical estimates, and analysis for the young, double-core, and obscured cluster Masgomas-4. The near-infrared observations, individual extinctions, and distance estimates for the OB-type star population are in agreement with a single association, with two active regions of stellar formation. The individual distances estimated for regions A and B point to a single distance of $1.90^{+1.28}_{-0.90}$ kpc, and this distance indicates that the cluster is associated with the IRAS source IRAS 18537+0753, the methanol maser [HHG86] 185345.9+074916, and the massive star forming region Sh2-76 E. The Algol variable star V 1665 Aql is discarded as part of the Masgomas-4 stellar population.

We observe in both regions A and B massive stars, and spectroscopic evidence of young or forming stars, like central stars 8a (emission Brackett series and Fe II at 1.64 μm in emission) and 9a (Fe II at 1.64 μm in emission). Regions A and B presents T Tauri candidates, according to their CCDs. In the case of region B, we also detect a clearly concentrated population of Herbig Ae/Be candidates around Sh2-76E. Its exclusive presence around the region B core could indicate a different star formation history between regions A and B (due to initial mass or age) and a slightly younger population in the region B core.

The mass estimate, derived from integrating the Kroupa initial mass function fitted to our data, gives a lower limit for the cluster total mass of $(2.19 \pm 0.31) \cdot 10^3$ $M_{\odot}$. The presence of T Tauri and Herbig Ae/Be candidates and the surrounding gas observed in mid-infrared images imply that Masgomas-4 is still a young and active object in terms of star formation. The very young obscured population and the surrounding gas allow us to limit the cluster age to less than 5 Myr.

Acknowledgements. S.R.A. was supported by the GEMINI-CONICYT project number 32110005, the FONDECYT project No. 3140605, and the investigation project Massive Stars in Galactic Obscured Massive Clusters. Part of this work was supported by the Science and Technology Ministry of the Kingdom of Spain (grants AYA2010-21697-C05-04 and AYA2012-39364-C02-01), the Gobierno de Canarias (PID2010119), and by the Chilean Ministry for the Economy, Development, and Tourism's Programa Inicativa Científica Milenio through grant IC 12009, awarded to The Millennium Institute of Astrophysics (MAS).

The William Herschel Telescope is operated on the island of La Palma by the Isaac Newton Group in the Spanish Observatorio del Roque de los Muchachos of the Instituto de Astrofísica de Canarias. This publication makes use of data products from the Two Micron All Sky Survey, which is a joint project of the University of Massachusetts and the Infrared Processing and Analysis Center/California Institute of Technology, funded by the National Aeronautics and Space Administration and the National Science Foundation. Average asymmetrical errors were estimated using the Java applet available in http://www.slac.stanford.edu/~barlow/statistics.html (Barlow 2004).

References

Alexander, M. J., Kobulnicky, H. A., Clemens, D. P., et al. 2009, AJ, 137, 4824
Barlow, R. 2004, [arXiv:physics/0406120]
Baudry, A., Desmurs, J. F., Wilson, T. L., & Cohen, R. J. 1997, A&A, 325, 255
Benjamin, R. A., Churchwell, E., Babler, B. L., et al. 2003, PASP, 115, 953
Bica, E., Dutra, C. M., & Barbuy, B. 2003a, A&A, 397, 177
Bica, E., Dutra, C. M., Soares, J., & Barbuy, B. 2003b, A&A, 404, 223
Borissova, J., Bonatto, C., Kurtev, R., et al. 2011, A&A, 532, A131
Brott, I., de Mink, S. E., Cantiello, M., et al. 2011, A&A, 530, A115
Chan, S. J., Henning, T., & Schreyer, K. 1995, VizieR Online Data Catalog, 411, 50285
Chan, S. J., Henning, T., & Schreyer, K. 1996, A&AS, 115, 285
Clark, J. S., Negueruela, I., Davies, B., et al. 2009, A&A, 498, 109

Comerón, F. & Pasquali, A. 2005, A&A, 430, 541
Cox, A. N. 2000, Allen's Astrophysical Quantities, 4th edition (Springer, New York)
Davies, B., Bastian, N., Gieles, M., et al. 2011, MNRAS, 411, 1386
Davies, B., Figer, D. F., Kudritzki, R.-P., et al. 2007, ApJ, 671, 781
Dutra, C. M., Bica, E., Soares, J., & Barbuy, B. 2003, A&A, 400, 533
Eikenberry, S., Elston, R., Raines, S. N., et al. 2006, in Ground-based and Airborne Instrumentation for Astronomy, ed. I. S. McLean, & M. Iye (SPIE, Washington), Proceedings of the SPIE, 6269, 626917
Figer, D. F., MacKenty, J. W., Robberto, M., et al. 2006, ApJ, 643, 1166
Forbes, D. 1989, A&AS, 77, 439
Fragoso-López, A. B., Acosta-Pulido, J. A., Hernández, E., et al. 2008, in Ground-based and Airborne Instrumentation for Astronomy II, ed. I. S. McLean, & M. M. Casali (SPIE, Washington), Proceedings of the SPIE, 7014, 701468
Froebrich, D., Scholz, A., & Raftery, C. L. 2007, MNRAS, 374, 399
González-Fernández, C. & Negueruela, I. 2012, A&A, 539, A100
Hanson, M. M., Conti, P. S., & Rieke, M. J. 1996, ApJS, 107, 281
Hanson, M. M., Kudritzki, R., Kenworthy, M. A., Puls, J., & Tokunaga, A. T. 2005, ApJS, 161, 154
Hanson, M. M., Kurtev, R., Borissova, J., et al. 2010, A&A, 516, A35
Hanson, M. M. & Popescu, B. 2008, in IAU Symposium, Vol. 250, IAU Symposium, ed. F. Bresolin, P. A. Crowther, & J. Puls, 307–312
Hanson, M. M., Rieke, G. H., & Luhman, K. L. 1998, AJ, 116, 1915
Hernández, J., Hartmann, L., Megeath, T., et al. 2007, ApJ, 662, 1067
Ibanoğlu, C., Evren, S., Taş, G., et al. 2007, MNRAS, 380, 1422
Kroupa, P. 2001, MNRAS, 322, 231
Kurtev, R., Borissova, J., Georgiev, L., Ortolani, S., & Ivanov, V. D. 2007, A&A, 475, 209
Kurtev, R., Ivanov, V. D., Borissova, J., & Ortolani, S. 2008, A&A, 489, 583
Lada, C. J. & Lada, E. A. 2003, ARA&A, 41, 57
Lawrence, A., Warren, S. J., Almaini, O., et al. 2007, MNRAS, 379, 1599
Manchado, A., Barreto, M., Acosta-Pulido, J., et al. 2004, in Ground-based and Airborne Instrumentation for Astronomy, ed. A. F. M. Moorwood, & M. Iye (SPIE, Washington), Proceedings of the SPIE, 5492, 549188
Marín-Franch, A., Herrero, A., Lenorzer, A., et al. 2009, A&A, 502, 559
Martins, F., Schaerer, D., & Hillier, D. J. 2005, A&A, 436, 1049
Mercer, E. P., Clemens, D. P., Meade, M. R., et al. 2005, ApJ, 635, 560
Meyer, M. R., Edwards, S., Hinkle, K. H., & Strom, S. E. 1998, ApJ, 508, 397
Minniti, D., Lucas, P. W., Emerson, J. P., et al. 2010, New Astronomy, 15, 433
Negueruela, I., González-Fernández, C., Marco, A., & Clark, J. S. 2011, A&A, 528, A59
Negueruela, I., González-Fernández, C., Marco, A., Clark, J. S., & Martínez-Núñez, S. 2010, A&A, 513, 74
Negueruela, I. & Schurch, M. P. E. 2007, A&A, 461, 631
Newberry, M. V. 1991, PASP, 103, 122
Palagi, F., Cesaroni, R., Comoretto, G., Felli, M., & Natale, V. 1993, A&AS, 101, 153
Plume, R., Jaffe, D. T., & Evans, II, N. J. 1992, ApJS, 78, 505
Puga, E., Marín-Franch, A., Najarro, F., et al. 2010, A&A, 517, A2
Ramírez Alegría, S., Herrero, A., Marín-Franch, A., et al. 2011, A&A, 535, A8
Ramírez Alegría, S., Marín-Franch, A., & Herrero, A. 2012, A&A, 541, A75
Ranade, A., Gupta, R., Ashok, N. M., & Singh, H. P. 2004, Bulletin of the Astronomical Society of India, 32, 311
Rieke, G. H. & Lebofsky, M. J. 1985, ApJ, 288, 618
Rieke, G. H., Rieke, M. J., & Paul, A. E. 1989, ApJ, 336, 752
Saito, R. K., Hempel, M., Minniti, D., et al. 2012, A&A, 537, A107
Sharpless, S. 1959, ApJS, 4, 257
Skrutskie, M. F., Cutri, R. M., Stiening, R., et al. 2006, AJ, 131, 1163
Slysh, V. I., Val'tts, I. E., Kalenskii, S. V., et al. 1999, A&AS, 134, 115
Stetson, P. B. 1994, PASP, 106, 250
Subramaniam, A., Mathew, B., Bhatt, B. C., & Ramya, S. 2006, MNRAS, 370, 743
Szymczak, M., Hrynek, G., & Kus, A. J. 2000, A&AS, 143, 269
Tokunaga, A. T. 2000, Infrared Astronomy (Springer), 143
Vacca, W. D., Cushing, M. C., & Rayner, J. T. 2003, PASP, 115, 389
Val'tts, I. E., Ellingsen, S. P., Slysh, V. I., et al. 2000, MNRAS, 317, 315
Wallace, L. & Hinkle, K. 1997, ApJS, 111, 445
Zinchenko, I., Forsstroem, V., Lapinov, A., & Mattila, K. 1994, A&A, 288, 601
Zinchenko, I., Henning, T., & Schreyer, K. 1997, A&AS, 124, 385

List of Objects

'V 1665 Aql' on page 2
'V 1665 Aql' on page 2
'HD 231033' on page 4
'V 1665 Aql' on page 11